J Shoulder Elbow Surg (2021) 30, 561–571

ELSEVIER

Journal of Shoulder and Elbow Surgery

www.elsevier.com/locate/ymse

Automated muscle elongation measurement during reverse shoulder arthroplasty planning

Jonathan Pitocchi, MSc[a,b,c,*,1], Katrien Plessers, MSc[a,c,1], Roel Wirix-Speetjens, PhD[a], Philippe Debeer, MD, PhD[d,e,f], G. Harry van Lenthe, PhD[c], Ilse Jonkers, PhD[g], Maria Angeles Pérez, PhD[b], Jos Vander Sloten, PhD[c]

[a]*Materialise, Heverlee, Belgium*
[b]*Multiscale in Mechanical and Biological Engineering (M2BE), University of Zaragoza, Zaragoza, Spain*
[c]*Biomechanics Section, KU Leuven, Leuven, Belgium*
[d]*Orthopaedics Section, University Hospitals Leuven, Leuven, Belgium*
[e]*Department of Development and Regeneration, KU Leuven, Leuven, Belgium*
[f]*Institute for Orthopaedic Research and Training, Leuven, Belgium*
[g]*Department of Biomedical Kinesiology, KU Leuven, Leuven, Belgium*

Background: Adequate deltoid and rotator cuff elongation in reverse shoulder arthroplasty is crucial to maximize postoperative functional outcomes and to avoid complications. Measurements of deltoid and rotator cuff elongation during preoperative planning can support surgeons in selecting a suitable implant design and position. Therefore, this study presented and evaluated a fully automated method for measuring deltoid and rotator cuff elongation.

Methods: Complete scapular and humeral models were extracted from computed tomography scans of 40 subjects. First, a statistical shape model of the complete humerus was created and evaluated to identify the muscle attachment points. Next, a muscle wrapping algorithm was developed to identify the muscle paths and to compute muscle lengths and elongations after reverse shoulder arthroplasty implantation. The accuracy of the muscle attachment points and the muscle elongation measurements was evaluated for the 40 subjects by use of both complete and artificially created partial humeral models. Additionally, the muscle elongation measurements were evaluated for a set of 50 arthritic shoulder joints. Finally, a sensitivity analysis was performed to evaluate the impact of implant positioning on deltoid and rotator cuff elongation.

Results: For the complete humeral models, all muscle attachment points were identified with a median error < 3.5 mm. For the partial humeral models, the errors on the deltoid attachment point largely increased. Furthermore, all muscle elongation measurements showed an error < 1 mm for 75% of the subjects for both the complete and partial humeral models. For the arthritic shoulder joints, the errors on the muscle elongation measurements were < 2 mm for 75% of the subjects. Finally, the sensitivity analysis showed that muscle elongations were affected by implant positioning.

Discussion: This study presents an automated method for accurately measuring muscle elongations during preoperative planning of shoulder arthroplasty. The results show that the accuracy in measuring muscle elongations is higher than the accuracy in indicating the muscle attachment points. Hence, muscle elongation measurements are insensitive to the observed errors on the muscle attachment points. Related to this finding, muscle elongations can be accurately measured for both a complete humeral model and a partial humeral model. Because the presented method also showed accurate results for arthritic shoulder joints, it can be used during preoperative shoulder arthroplasty planning, in which typically only the proximal humerus is present in the scan and in which bone arthropathy can be present. As the muscle elongations are sensitive to implant positioning, surgeons can use the muscle elongation measurements to refine their surgical plan.

Institutional review board approval was not required for this basic science study.

[1] Joint first authors.

*Reprint requests: Jonathan Pitocchi, MSc, Materialise, Technologielaan 15, B-3001 Heverlee, Belgium.
E-mail address: jonathan.pitocchi@materialise.be (J. Pitocchi).

https://doi.org/10.1016/j.jse.2020.07.007

Level of evidence: Basic Science Study; Computer Modeling

Keywords: Statistical shape model; reverse shoulder arthroplasty; shoulder planning; muscle elongation; implant positioning; automatization

Adequate deltoid and rotator cuff tensioning in reverse shoulder arthroplasty (RSA) is crucial to maximize postoperative functional outcomes and to avoid complications.[12,15,35] Insufficient muscle tension can lead to instability problems and limited range of motion.[15,20,35] Over-tensioning the deltoid muscle can result in acromial fractures, a complication with an incidence of 1%-7%.[2,7,9,36] Because muscle tension is affected by muscle length, deltoid and rotator cuff elongations should be taken into account during preoperative planning of RSA procedures.

Not only implant design and position but also patient anatomy has an important impact on the muscle elongations following RSA procedures.[15] Several studies have investigated the effects of implant design and positioning on muscle elongations. Roche et al[28] evaluated the impact of implant design and placement on muscle elongations using a musculoskeletal shoulder model and reported more anatomic muscle tension with lateralization of the humerus. Wright et al[37] quantified deltoid elongation for 3 different baseplate positions during cadaveric testing and found that an inferior baseplate position increases the deltoid muscle length. Lädermann et al[14] showed that rotator cuff lengthening is affected by the glenoid implant configuration while observing the largest rotator cuff elongation when performing bony increased-offset (BIO) RSA. Although the impact of implant design and positioning on muscle elongations has been studied, a high level of uncertainty on how to ensure adequate muscle elongation during preoperative RSA planning still exists among surgeons.[28] Indications of deltoid and rotator cuff elongations as part of preoperative RSA planning can support surgeons in evaluating muscle tension and refining their surgical plan accordingly.[35]

To measure deltoid and rotator cuff elongations during preoperative planning, an accurate—and preferably automated—measurement method is desired. Therefore, accurate identification of patient-specific muscle attachment and wrapping points is required. Manual indication of muscle attachment sites on the images or 3-dimensional (3D) models is time-consuming and subject to interobserver variability.[10,35] Automated methods have been reported that transfer the muscle attachment and wrapping points from one bone model to another by defining a transformation matrix between the bone models.[13,16,24,27] However, the accuracy of these transformation or morphing methods can be limited for bone models with more distinct shapes.[24] Moreover, the reported morphing algorithms have difficulties with incomplete bone shapes. This is problematic in the case of preoperative shoulder arthroplasty planning, as the medical images typically contain only the proximal humerus.[13,24] More recently, machine learning–based methods have been introduced to automatically detect multiple landmarks in medical images.[21,23,38] Although promising results have been shown, the accuracy of these approaches is dependent on the amount of data used for training. Additionally, only landmarks actually present on the images can be identified, thus limiting the applicability of these methods to medical images with the muscle attachment points within the field of view of the scan.

Several studies have shown the potential of statistical shape modeling for automated landmark prediction based on partial or complete bone models.[25,26,31,33] Statistical shape models (SSMs) are fitted to a target bone model, thereby better maintaining point correspondence and being less dependent on bone shape in comparison to morphing methods. Salhi et al[29] evaluated the prediction accuracy of muscle attachment regions on the scapula and humerus using an SSM approach. Although good accuracy was reported, the study used only a limited evaluation data set and did not report the errors that can be expected on muscle elongation measurements. Therefore, the goal of our study was to develop and evaluate the accuracy of an automated method for measuring deltoid and rotator cuff elongation during preoperative planning of RSA based on an SSM approach. The presented method consists of a landmark identification landmarking algorithm to identify the muscle attachment points and a wrapping algorithm to identify the path of each muscle around the bones and implants. Once the muscle paths were known, muscle elongation was defined as the change in muscle length relative to the preoperative joint state. Because preoperative shoulder arthroplasty images typically contain only the proximal humerus, the accuracy of the muscle attachment points and muscle elongation measurements was evaluated for both complete and partial humeral models. Additionally, the automated workflow accuracy was evaluated for a data set of arthritic shoulder joints, used for preoperative planning of shoulder arthroplasty. Finally, a sensitivity study was performed to demonstrate the effect of implant positioning on muscle elongations.

Materials and methods

Data

We selected a set of 40 computed tomography (CT) scans with a complete scapula and humerus to evaluate the muscle elongation

measurements. The average slice spacing of the acquired images was 0.5 mm. The set included 25 men and 15 women, with an average age of 63 years. All selected scapulae and humeri showed no significant signs of bone defect or arthropathy. The scans were manually segmented by Mimics image processing software (version 20; Materialise, Leuven, Belgium) and converted into 3D models, with a mean triangular edge length of 1.5 mm for the scapulae and 2 mm for the humeri. To simulate the presence of an incomplete humerus in the scan and evaluate its impact on the presented method, partial humeral models were created from the 40 complete humeral models by artificially cutting the bone to 30% length from the top.

For indication of the muscle attachment points, SSMs of the scapula and humerus were required. A scapular SSM was already presented in a previous study.[25] This SSM included 66 three-dimensional models of healthy scapulae and was used to successfully reconstruct glenoid bone defects. The scapular models were segmented from CT scan images and showed no signs of bone defect or arthropathy (cysts, osteophytes, or sclerosis). For the humerus, a new SSM was built based on the same 40 complete humeral models that were used for evaluation. The creation of the SSM is described later.

To assess the accuracy of the automated workflow on arthritic joints, 50 CT scans were randomly selected from a data set of images used for preoperative planning of shoulder arthroplasty. All scapulae and humeri showed signs of bone defect or arthropathy. The scans had an average slice spacing of 0.6 mm and were acquired with different machine parameters. By use of Mimics software (version 20), the scapula and proximal humerus were converted into 3D bone models with mean triangular edge lengths of 1.5 mm and 2 mm, respectively.

Anatomic landmarks

We identified 11 anatomic landmarks on the scapula and 6 on the humerus. On the scapula, the subscapularis, supraspinatus, and infraspinatus attachment points were located centrally and close to the medial side of the subscapularis, supraspinatus, and infraspinatus fossa, respectively (Fig. 1). The teres minor attachment point was defined in the middle of the scapula's lateral rim. The middle and posterior deltoid attachment points were located at the tip of the acromion and at the middle of the scapular spine, respectively. Furthermore, the scapular coordinate frame was defined by the glenoid center point (center of mass of all points on the glenoid surface), trigonum spinae (midpoint of the triangular surface on the medial border), and angulus inferior (most inferior point).[8,25] To compute the wrapping of the muscles, 2 additional landmarks were identified: the acromial and coracoid neck points.

On the humerus, the supraspinatus, infraspinatus, and teres minor attachment points were located on the anterior, lateral, and posterior sides of the greater tubercle, respectively (Fig. 2). The subscapularis attachment point was defined on the middle of the lesser tubercle. Because the deltoid tuberosity was not clearly visible on the humeral model, the deltoid attachment point was identified at 50% of the humeral length and above the lateral epicondylar point, consistent with what has been reported in cadaveric studies in the literature.[19,22] The deltoid attachment point on the humerus was the attachment point for both the middle and posterior deltoid.

Humeral SSM

To create a humeral SSM, the muscle attachment points and epicondylar points were manually indicated on the 40 complete humerus models by 2 experts (J.P. and K.P). The deltoid attachment point was derived from the lateral epicondylar point, as described previously. The mean landmark positions of the 2 observers were projected onto the surface of the humeral model to obtain the final landmark positions. These final landmarks served as inputs for creation of the humeral SSM. Interobserver variability was computed for all muscle attachment points as the distance from the observed landmark position to the mean landmark position.[34]

On the basis of the 40 complete humeral models and indicated landmarks, an SSM was created (Python, version 3.7; Python Software Foundation, Wilmington, DE, USA). To capture the variation between the models, all humeral models required corresponding points. To solve the corresponding-point problem, one model of the data set was registered as a template to all other models.[25,33] First, the template was aligned to the other models using an iterative closest point (ICP)

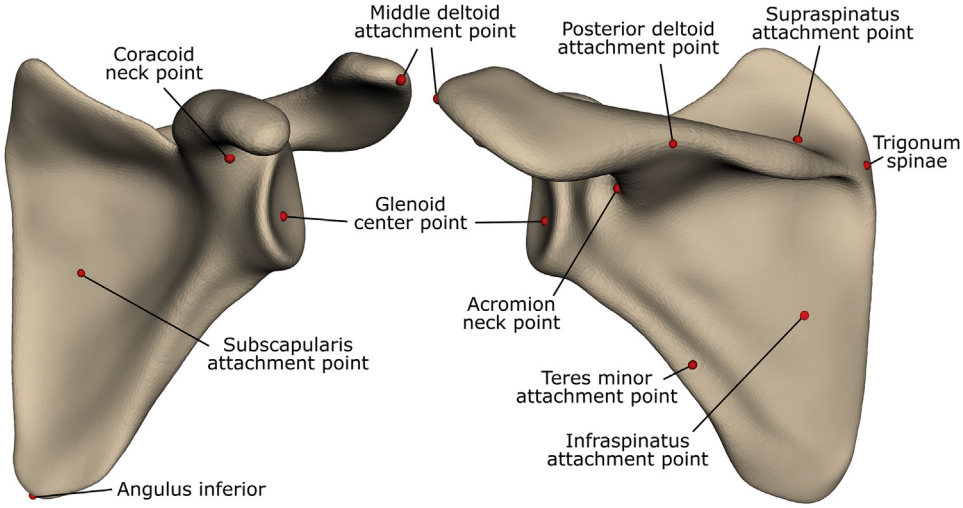

Figure 1 Anatomic landmarks on scapula.

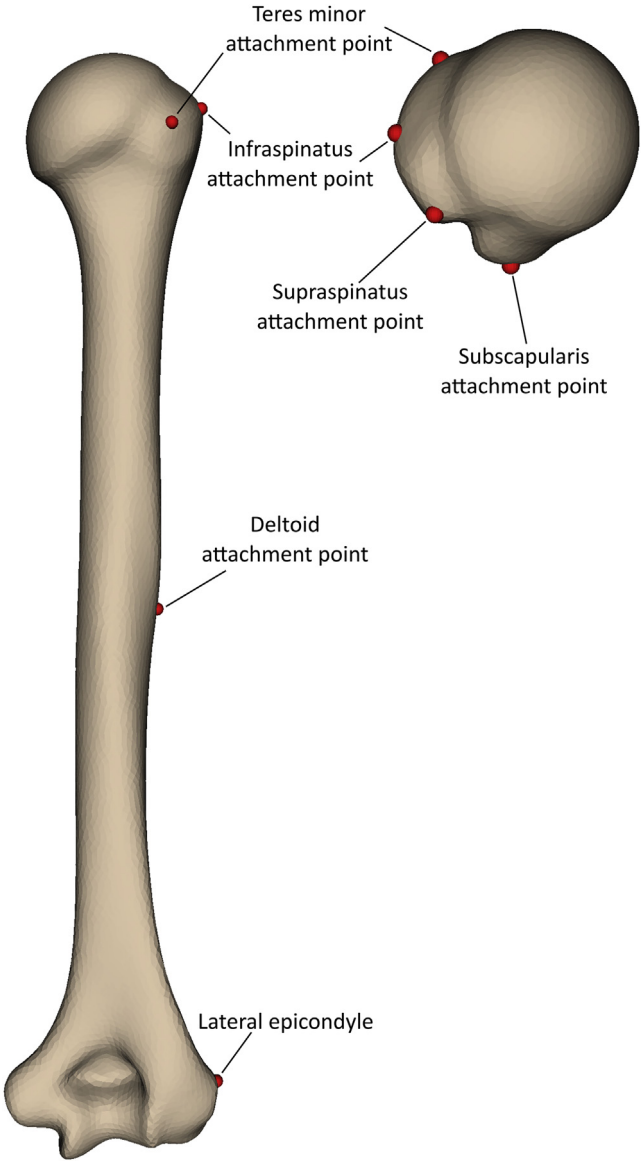

Figure 2 Anatomic landmarks on humerus.

algorithm without scaling. Then, a thin plate spline (TPS) registration algorithm[32] was applied using the manually indicated landmarks to guide the shape deformation of the template to the other models. Next, an elastic surface registration algorithm, as described by Danckaers et al,[6] was applied to fine-tune the shape deformation. After registration, all models were aligned by excluding the translational and rotational variations using a Procrustes algorithm without scaling. Finally, a principal component analysis was performed to extract the mean shape and the different modes of variation.[5]

Automated landmark identification

The muscle attachment points and coordinate frames could be automatically identified on a target shape using an SSM.[25,33] The required landmarks were manually indicated on the mean SSM shape and then transferred to the target shape by registering and fitting the SSM. For the scapula, the registration and fitting method was described in a previous study.[26] Via an iterative approach, the mean SSM shape was registered to the target scapular shape, corresponding points were identified, and the SSM coefficients were computed by adapting the SSM shape to match the identified corresponding points (Python, version 3.7).

For the humerus, the registration and fitting methods were adapted to account for the axisymmetrical shape of the humerus and to include scans that contained only the proximal humerus. The adapted registration method consisted of 2 steps (Fig. 3): First, the mean shape of the SSM was cut by planes at different heights, and each resulting proximal mean shape was aligned to the target shape using an inertia registration. Uniform scaling was applied to account for the difference in size. Between all the cutting planes, the one that minimized the root-mean-square (RMS) of the distances between the proximal mean shape and the target shape was selected. Second, the selected proximal mean shape was iteratively rotated around its long axis and registered to the target model through an iterative closest point (ICP) algorithm to find the rotation angle that minimized the RMS of the distances. This second step enforced good alignment despite the axisymmetrical shape of the humerus.

After the registration, the SSM was fitted to the target humeral shape. The fitting method, as described in a previous study,[26] was adapted to ignore points that were lying under the selected cutting plane, as obtained from step 1 of the registration. Hence, these points were excluded from the corresponding point search of the fitting method so that only the information present in the scan was taken into account.

After fitting the SSM, the muscle attachment points were projected from the fitted SSM shape onto the target scapular and humeral shape. Because the CT scans of some patients contained only the proximal part of the humerus, the deltoid attachment point could not always be projected onto the target humerus because in these cases the corresponding surface was not available. Therefore, the deltoid attachment point was only projected onto the target humeral shape if it was lying above the cutting plane obtained from the registration method (Fig. 3). This meant that the deltoid attachment point could be floating if only the proximal humerus was present in the scan.

Muscle length measurement

Once the muscle attachment points were identified, the rotator cuff and deltoid paths could be computed. Similarly to existing musculoskeletal models,[11,30] each muscle was represented by a line trajectory (Fig. 4). The rotator cuff was visualized by 4 line trajectories: supraspinatus, infraspinatus, subscapularis, and teres minor. The deltoid muscle was shown by 2 line trajectories: middle deltoid and posterior deltoid. The anterior deltoid was excluded in this study to avoid the need for a 3D model of the clavicle.

A wrapping algorithm was used to identify the wrapping points forcing the muscle to wrap around the bones and potential implants (Python, version 3.7) (Fig. 5). This wrapping algorithm is a recursive algorithm that identifies the most distant point from the muscle line segment in a specific direction. This direction was obtained as follows: first, a fixed wrapping direction was defined for each muscle (Fig. 5, *a*). For the supraspinatus, infraspinatus, subscapularis, teres minor, middle deltoid, and posterior deltoid,

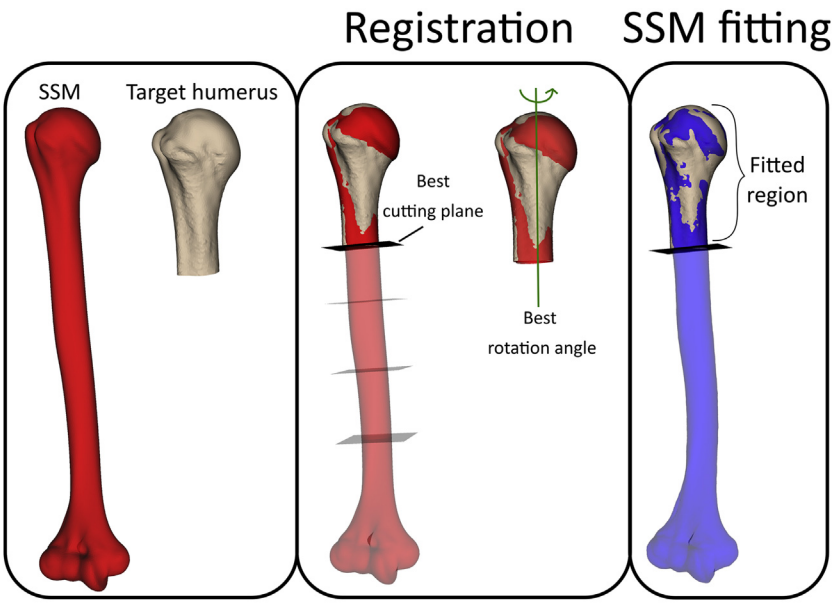

Figure 3 Workflow for registration and fitting of humeral statistical shape model *(SSM)* to target humeral shape. The target humeral shape can contain the complete humerus or only the proximal part (*left*). First, the best cutting plane and best rotation angle are selected to register the SSM to the target humeral shape (*middle*). Second, the SSM is fitted to the target humeral shape while all SSM points that are below the selected cutting plane are ignored (*right*).

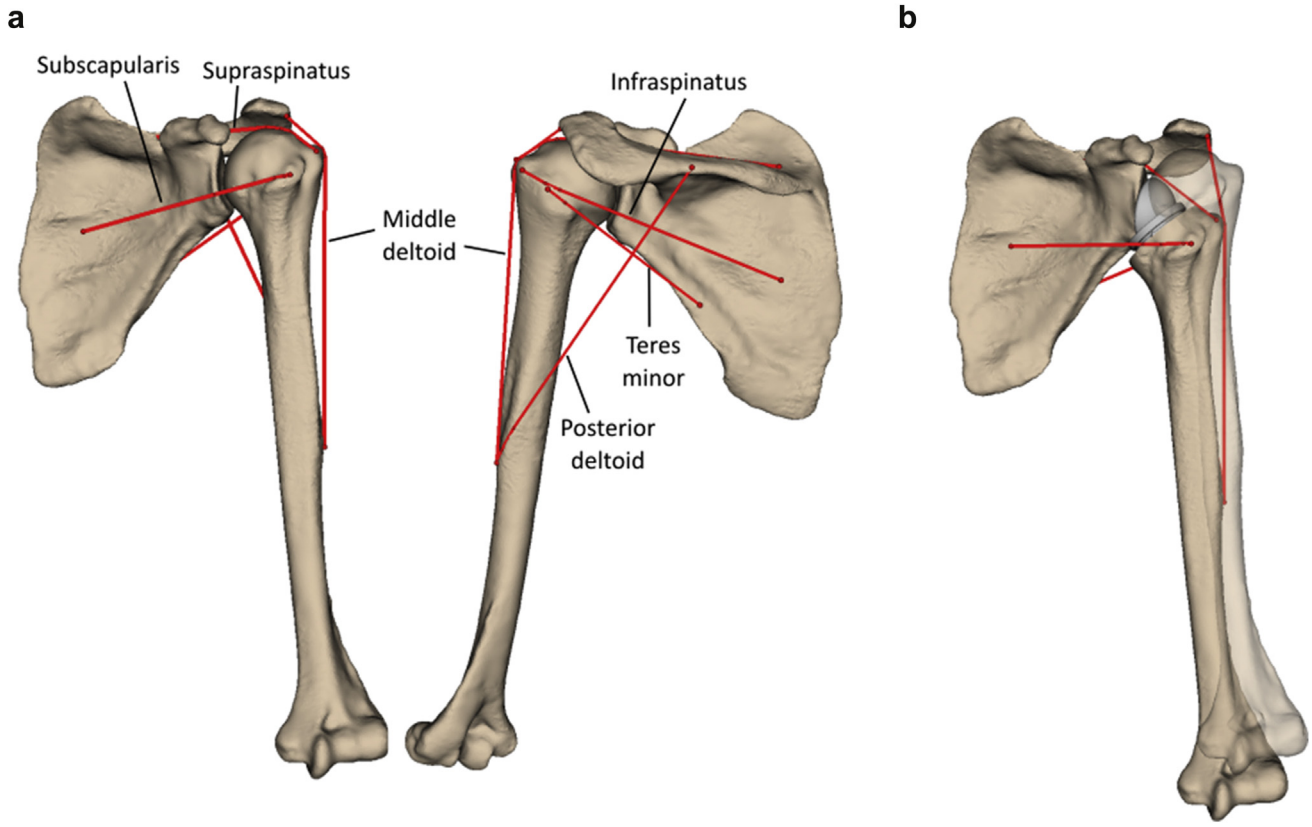

Figure 4 Rotator cuff and deltoid visualization for preoperative situation (**a**) and with planned shoulder arthroplasty (**b**) Muscle elongation is defined as the difference in length between the planned and preoperative situations.

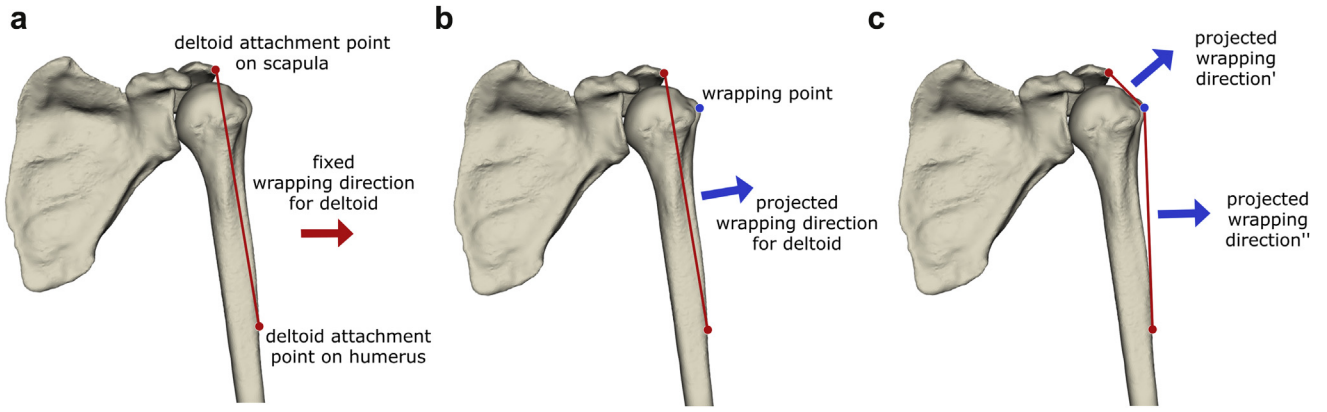

Figure 5 Wrapping algorithm. (**a**) For every muscle, a fixed wrapping direction is defined. (**b**) The fixed wrapping direction is projected onto the plane perpendicular to the muscle line, and the farthest point along this projected wrapping direction is identified as the wrapping point. (**c**) The muscle line is split into 2 separate line segments, and the wrapping algorithm is recursively applied to each of these segments.

the fixed wrapping directions were superior, posterior, anterior, posterior, lateral, and posterolateral, respectively, relative to the scapular coordinate frame. Then, this fixed wrapping direction was projected onto the plane, perpendicular to the muscle line (Fig. 5, *b*). Hence, the wrapping algorithm looked for the most distant point on the bones or implants along this projected wrapping direction. After identification of this wrapping point, the muscle was split into 2 separate line segments and the algorithm was applied to both segments separately, until no more points could be found along the projected wrapping direction (Fig. 5, *c*).

To avoid wrapping of the supraspinatus and subscapularis around the acromion and coracoid, the acromial and coracoid surfaces were cut off before the wrapping algorithm was started. All points of the scapular model that were lying superior and posterior to the acromial neck landmark or superior, anterior, and lateral to the coracoid neck landmark, measured in the scapular coordinate frame, were not taken into account in the calculation.

When the muscle path was known, the muscle length was computed as the sum of the lengths of the different line segments. Muscle elongation was defined as the difference in muscle length between the preoperative situation (no implant) and the postoperative or planned situation, in which a shoulder arthroplasty has been (virtually) implanted (Fig. 4).

Evaluation of humeral landmark identification accuracy

The accuracy of the automatically identified humeral landmarks and their effect on muscle length and elongation measurements were evaluated by comparing the manually indicated landmarks with the automatically identified landmarks for the set of 40 scapular and humeral models. First, the muscle attachment points on all 40 scapular and humeral models were automatically identified by fitting the SSMs and projecting the landmarks, as previously explained. Because the humeral SSM was created from the same data used for the evaluation data set, a leave-one-out cross validation was performed. For each selected humerus, a new "sub"-SSM was created from all 39 remaining humeri while excluding the selected humerus. This evaluation was repeated for all 40 humeri. After identification of the muscle attachment points, additional wrapping points were determined and the muscle lengths were computed. Next, reverse humeral and glenoid implants (DePuy Synthes, Warsaw, IN, USA) were virtually implanted. For all subjects, glenoid and humeral implants (38-mm glenosphere) were positioned in a fixed position. The glenoid metaglene was positioned 5 mm below the glenoid center point and in 0° of inclination and version relative to the mediolateral axis of the scapula.[1,3] The humeral implant was positioned along the humeral shaft, with 30° of retroversion. The muscle lengths were recomputed, and the muscle elongations relative to the preoperative situation were calculated. Finally, the muscle length and elongation measurements were repeated for all subjects using the manually indicated landmarks and compared with the results obtained with the automatically indicated landmarks. To evaluate the accuracy for patients with incomplete humeri in the scan, each humerus was cut to 30% length from the top and the automated landmark indication and muscle measurements were repeated. A paired *t* test was performed to investigate whether there was a statistically significant ($P < .05$) difference in the results between the complete and partial (30%) humeri.

Because the scapular SSM and fitting method showed good accuracy for the prediction of anatomic landmarks in a previous study[25] (mean error on glenoid center point, 1.8 mm), the accuracy of the scapular muscle attachment points and its effect on the muscle measurements were not evaluated in this study.

Application to arthritic joints

To assess the accuracy of the muscle elongation measurements on arthritic joints, the automated workflow was evaluated for a set of 50 arthritic scapular and humeral models. Because the humeral models contained only the proximal part of the humerus, the middle deltoid and posterior deltoid were excluded from the evaluation. First, the muscle attachment points on all humeral models were manually indicated by 2 experts (J.P. and K.P.), reaching consensus, and automatically indicated by fitting the SSMs and projecting the landmarks, as previously explained. Then, all bone models were virtually implanted with a reverse humeral and glenoid implant (DePuy Synthes). Finally, muscle elongations were measured with the manually indicated landmarks and with the automatically indicated landmarks, and the results were compared between the 2 methods.

Sensitivity analysis

To demonstrate the use of muscle length measurements during preoperative planning, a sensitivity study was performed on the set of 40 complete scapular and humeral models. The effect of implant positioning on muscle elongation was evaluated by subsequently translating the glenoid baseplate 5 mm more lateral and the humeral implant 5 mm more superior. In addition, the effect of implant orientation was investigated by subsequently rotating the glenoid baseplate 10° more retroverted and the humeral implant 10° more anteverted (resulting in 20° of humeral retroversion). For each position and orientation of the implants, muscle elongations were measured for the 4 rotator cuff muscles and the 2 deltoid muscles. Because RSA is more frequently being used with an intact rotator cuff, no muscles were excluded from the sensitivity analysis.[4,18]

Results

The interoperator error for the subscapularis, supraspinatus, infraspinatus, and teres minor attachment points on the humerus showed median values of 0.8 mm (interquartile range [IQR], 0.4-1.2 mm), 0.5 mm (IQR, 0.3-0.7 mm), 1.2 mm (IQR, 0.6-2.0 mm), and 1.2 mm (IQR, 0.6-3.0 mm), respectively (Fig. 6). The deltoid attachment point, which is derived from the lateral epicondylar point, resulted in median interobserver variability of 0.1 mm (IQR, 0.0-0.2 mm).

When the landmarks were automatically indicated on the complete humeral models using the SSM, median error values of 1.8 mm (IQR, 1.1-2.9 mm), 1.9 mm (IQR, 1.3-2.7 mm), 2.2 mm (IQR, 1.1-4.0 mm), 3.5 mm (IQR, 1.8-5.0 mm), and 0.8 mm (IQR, 0.6-1.2 mm) were observed for the muscle attachment points of the subscapularis, supraspinatus, infraspinatus, teres minor, and deltoid, respectively. For the partial humeral models, the errors resulted in median values of 1.8 mm (IQR, 1.2-2.8 mm), 1.6 mm (IQR, 1.2-2.3 mm), 2.1 mm (IQR, 1.5-3.3 mm), 3.0 mm (IQR, 2.0-4.9 mm), and 8.6 mm (IQR, 5.3-11.9 mm), respectively. Only for the deltoid attachment point was a significant ($P < .05$) difference found in the results between the complete and partial (30%) humeri.

By use of the complete humeral models, muscle elongations after RSA implantation were predicted by the SSM with an error (median) of 0.3 mm (IQR, 0.1-0.4 mm), 0.6 mm (IQR, 0.3-1.0 mm), 0.2 mm (IQR, 0.1-0.6 mm), and 0.4 mm (IQR, 0.1-0.8 mm) for the subscapularis, supraspinatus, infraspinatus, and teres minor, respectively (Fig. 7). For the middle and posterior deltoid, the median and IQR of the errors were $\leq$0.1 mm. When the partial humeral models were used, no significant ($P < .05$) differences were observed in the muscle elongation errors, except for those of the deltoid. The median error values for middle and posterior deltoid elongation increased to 0.1 mm (IQR, 0.0-0.2 mm) and 0.8 mm (IQR, 0.5-1.7 mm), respectively.

When the automated workflow was applied to arthritic shoulder joints, muscle elongations were predicted by the SSM with an error (median) of 0.5 mm (IQR, 0.2-1 mm), 1.1 mm (IQR, 0.6-1.9 mm), 0.5 mm (IQR, 0.2-1.1 mm), and 0.6 mm (IQR, 0.3-1.2 mm) for the subscapularis, supraspinatus, infraspinatus, and teres minor, respectively (Fig. 8).

As shown by the sensitivity study, muscle elongations were affected by implant positioning (Table I). With the initial position of the glenoid and humeral implants, the subscapularis, infraspinatus, and teres minor showed a shortening, or negative elongation, compared with the preoperative situation, with median values of –15 mm, –23 mm, and –26 mm, respectively. The middle deltoid and posterior deltoid were elongated in all subjects, with a median value of 19 mm. The supraspinatus showed a

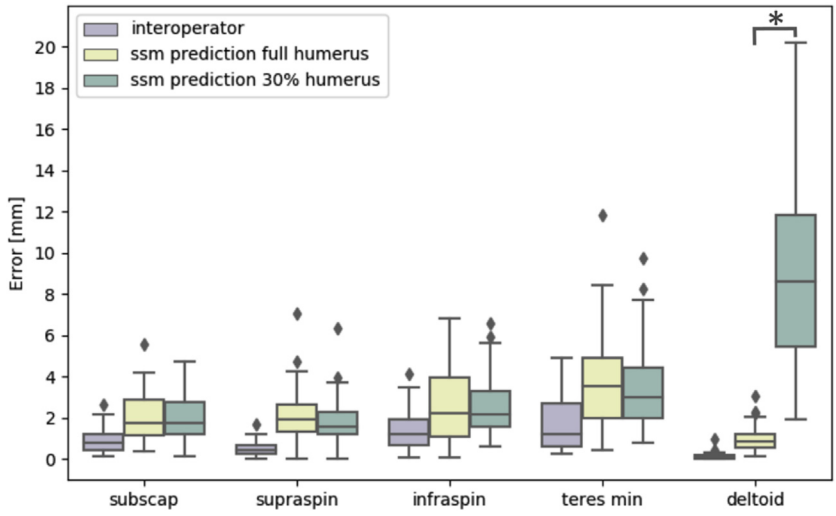

Figure 6 Interoperator and statistical shape modeling prediction errors on muscle attachment points of subscapularis (*subscap*), supraspinatus (*supraspin*), infraspinatus (*infraspin*), teres minor (*min*), and deltoid. The statistical shape model (*ssm*) prediction errors are computed for a complete humerus and partial (30%) humerus. *Statistically significant ($P < .05$) difference.

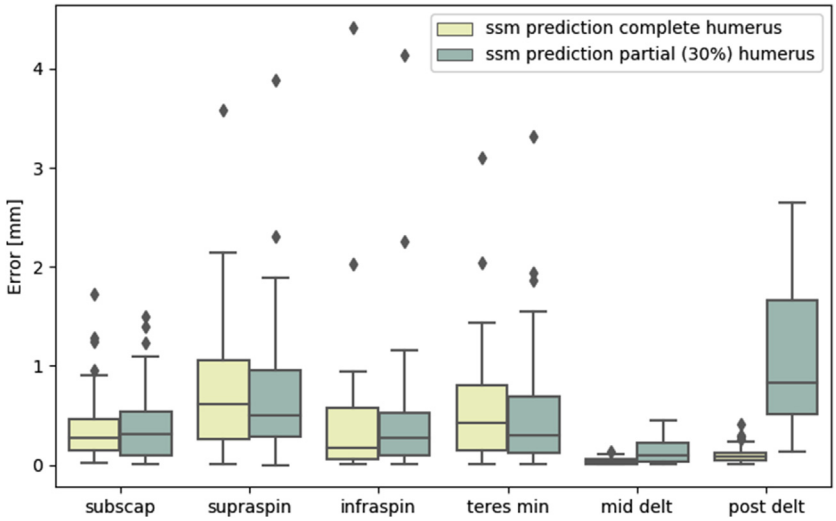

Figure 7 Statistical shape modeling prediction errors on muscle elongations of subscapularis (*subscap*), supraspinatus (*supraspin*), infraspinatus (*infraspin*), teres minor (*min*), middle deltoid (*mid delt*), and posterior deltoid (*post delt*). The statistical shape model (*ssm*) prediction errors are computed for a complete humerus and partial (30%) humerus.

median of 0 mm of elongation. Translating the glenoid implant 5 mm more lateral stretched the rotator cuff muscles compared with the default implant position, with a median value of 4-5 mm. Deltoid elongation only slightly increased with lateral translation of the glenoid implant. When the humeral implant was positioned 5 mm more superior, corresponding to an inferior offset of the humeral bone, deltoid elongation increased from a median of 19 mm to 24 mm compared with the initial implant position. Rotator cuff elongations, however, were only minimally affected by a more superior humeral implant position. Finally, changing the retroversion of the humeral and glenoid implant showed a limited effect on the muscle elongations.

Discussion

Estimates of deltoid and rotator cuff elongation can support surgeons during preoperative shoulder arthroplasty planning in selecting an implant design and position resulting in adequate muscle tension. Therefore, this study presented and evaluated a fully automated method to accurately measure deltoid and rotator cuff elongations, thus eliminating the need for time-consuming manual interactions. Because preoperative shoulder arthroplasty images typically contain only the proximal humerus, the method was evaluated for both complete and partial humeri. To evaluate its use in a clinical setting, the method was additionally applied to a set of arthritic shoulder joints.

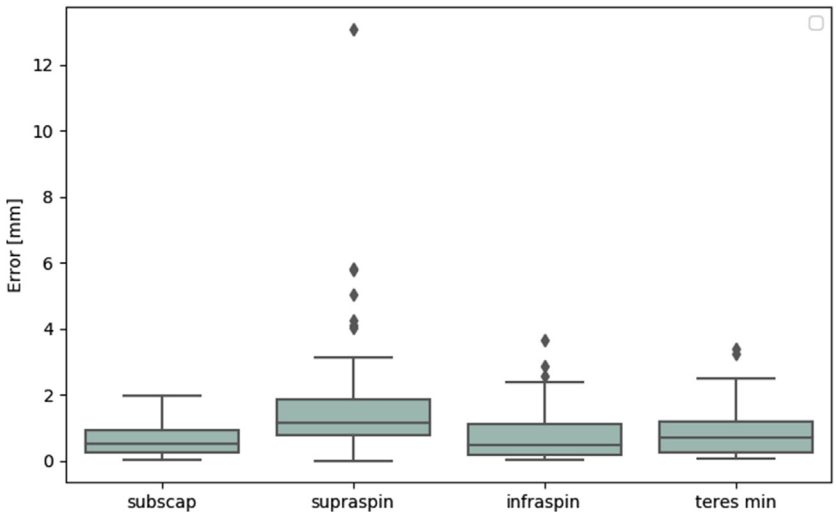

Figure 8 Statistical shape modeling prediction errors on muscle elongations for arthritic joints. Results are reported for the subscapularis (*subscap*), supraspinatus (*supraspin*), infraspinatus (*infraspin*), and teres minor (*min*), with the deltoid attachment point on the humerus being out of the scan field of view.

Table I Effect of implant position on muscle elongation measurements

	Subscapularis, mm	Supraspinatus, mm	Infraspinatus, mm	Teres minor, mm	Middle deltoid, mm	Posterior deltoid, mm
Initial implant position	−15 (−21 to −13)	0 (−8 to 2)	−23 (−27 to −21)	−26 (−29 to −24)	19 (15 to 23)	19 (16 to 22)
Glenoid implant positioned +5 mm lateral	−10 (−17 to −8)	4 (−4 to 6)	−19 (−23 to −16)	−22 (−25 to −19)	20 (17 to 24)	22 (17 to 24)
Humeral implant positioned +5 mm superior	−15 (−21 to −12)	3 (−5 to 6)	−23 (−28 to −21)	−27 (−31 to −25)	24 (20 to 28)	24 (20 to 27)
Humeral implant with −10° of retroversion	−16 (−22 to −12)	−1 (−9 to 3)	−22 (−26 to −19)	−25 (−28 to −22)	18 (15 to 22)	19 (16 to 22)
Glenoid implant with +10° of retroversion	−15 (−21 to −13)	0 (−8 to 2)	−23 (−27 to −21)	−26 (−29 to −24)	18 (15 to 23)	19 (16 to 22)

Data are reported as median (interquartile range).

First, the method was evaluated for automated identification of the muscle attachment points in a set of 40 complete humeral models. The errors for the automatically identified landmarks were higher than the interoperator errors for all landmarks. This was partly because of the accuracy of the SSM landmarks being limited by the 2-mm SSM mesh size. To clarify, the landmarks on the SSM were linked to the nodes of the SSM mesh whereas the operators were allowed to put landmarks between the nodes. Furthermore, a correlation was observed between the interobserver errors and the automatic landmark identification errors. Landmarks that were indicated less consistently, such as the teres minor and infraspinatus, showed higher automatic landmark identification errors than the other landmarks.

For the partial humeral models, the automatic landmark identification errors slightly decreased for the subscapularis, supraspinatus, infraspinatus, and teres minor attachment points. Because the SSM is fitted to a smaller surface, it better optimizes its shape toward this small surface, resulting in a more accurate indication of the landmarks. However, for the deltoid attachment point, the automatic landmark identification errors largely increased when only the proximal humerus was available. These large errors are a result of the lack of information related to the distal humerus, which is not taken into account when fitting the SSM. Because the deltoid attachment point is defined by the lateral epicondylar point and the humeral length, the distal shape of the humerus is important for accurately predicting its position.

The SSM-based landmark identification algorithm performs better than alternative methods reported in the literature. Pellikaan et al[24] investigated the accuracy of a morphing method to transform the muscle attachment regions between 2 cadaveric legs. They reported morphing errors with a median $>$ 10 mm for all muscle attachment regions, which is higher than the median values of 0.8-3.5 mm that we measured on the muscle attachment points. Kaptein and van der Helm[13] evaluated a similar morphing method on the muscle attachment regions of the shoulder bones. They obtained a median of 7 mm for morphing errors. Other methods to transform the muscle attachment points from one bone to another include linear scaling and nonlinear scaling.[17] These methods also were found to perform less accurately than the SSM-based landmark identification algorithm presented in our study.[17,24]

Our results are comparable to those of other SSM-based landmark identification methods described in the literature. Salhi et al[29] investigated the prediction accuracy of subject-specific muscle attachment regions using a healthy scapular and humeral SSM. For the humerus, they reported an average RMS error between 0.4 and 1.7 mm and a Hausdorff distance between 1.6 and 4.8 mm for all muscle attachment regions. Similarly to our results, the muscles followed the same descending order of accuracies, going from the subscapularis to the supraspinatus, infraspinatus, and teres minor. In contrast to our study, Salhi et al did not evaluate the prediction accuracy when only 30% of the humerus was available in the scan.

Next, the presented method was evaluated for measuring muscle elongations following RSA. When an RSA was virtually implanted, muscle elongations were predicted with errors $<$ 1 mm for 75% of the subjects. These errors are lower than the errors on the muscle attachment points. As a result, the relative changes in muscle lengths between the planned and preoperative situations can be computed more accurately than the exact location of the muscle attachment points. Hence, the muscle elongation measurements are insensitive to errors on the muscle attachment points. Because the impact of implant positioning on muscle elongations is generally $>$1 mm, we conclude that the muscle elongation measurements are sufficiently accurate for use during preoperative shoulder arthroplasty planning. For the partial (30%) humeral models, the errors on rotator cuff and middle deltoid elongation remained $<$1 mm for 75% of the subjects. Only for the posterior deltoid did the error (median) increase to 0.8 mm (IQR, 0.5-1.7 mm) when a partial humeral model was used. When applied to the set of 50 arthritic

shoulder joints, the automated workflow reported slightly higher error predictions, with values still <2 mm for 75% of the subjects. As we believe that these errors are still acceptable for clinical decision making, muscle elongation measurements can be applied in a clinical setting in which the scapula and humerus can show signs of bone defect and in which no complete model of the humerus needs to be present.

Finally, the sensitivity analysis confirmed the effects of implant positioning on muscle elongation measurements, in line with the results of other studies in the literature. As reported by Roche et al,[28] lateralization of the glenoid component increases the length of the rotator cuff muscles; this was also seen in our study. Lädermann et al[14] observed approximately 8 mm more elongation for all muscles when performing a bony increased-offset RSA with a 10-mm lateral offset instead of a normal RSA. Similarly to our results, Wright et al[37] observed increased deltoid elongation when using increasing inferior offsets. The fact that glenoid and humeral implant retroversion had a limited effect on the muscle elongation measurements can be explained by the unaltered orientation of the humerus relative to the scapula. Although retroversion changes the orientation of the implant in the bone, the orientation of the humerus relative to the scapula remains the same.

This study has some limitations. First, although the automated workflow was tested on arthritic joints, the accuracy of the middle and posterior deltoid muscle could not be assessed because its attachment point on the humerus was out of the scan field of view. Second, we did not evaluate the accuracy of the automatically indicated scapular landmarks. Because the scapular SSM and fitting method showed good accuracy for the prediction of landmarks and measurements in previous studies,[25,26] we did not re-evaluate this ability for the current muscle attachment points. Moreover, as demonstrated by Salhi et al,[29] the muscle attachment points on the scapula are expected to be indicated with higher accuracy than the muscle attachment points on the humerus because of the more distinct anatomic regions of the scapula. Third, we defined the muscle attachment points instead of using the complete muscle attachment regions. Although muscle attachment regions are a more accurate representation than points, the muscle attachment points are required to represent the individual line trajectory of the muscle. This approach is comparable to approaches in other studies that measured muscle lengths.[28,35] In addition, the exact location of the muscle attachment point has a limited impact on the muscle elongation measurements, as demonstrated in this study. Finally, the quality of the soft tissues was not taken into account. Therefore, it might be that the preoperatively selected elongations are not feasible and that the muscles do not accept these elongations during surgery. Despite this limitation, measuring muscle elongations during preoperative planning of shoulder arthroplasty is a first step toward integrating soft tissue information and supporting surgeons in selecting a suitable implant design and position.

Conclusion

This study presents an automated method for accurately measuring muscle elongations during preoperative planning of shoulder arthroplasty. The method was able to measure rotator cuff and deltoid elongation with an error < 1 mm for 75% of the subjects. Only the errors on the posterior deltoid increased when 30% of the complete humerus was present in the scan. Muscle elongation errors for the arthritic joints were <2 mm for 75% of the subjects. As a result, the presented method can be applied in a clinical setting despite the fact that medical images for shoulder arthroplasty typically contain only the proximal humerus and bones can show signs of arthropathy. Moreover, the sensitivity analysis showed that the measurements are affected by implant positioning and thus can support surgeons in evaluating and refining their surgical plan during preoperative planning of shoulder arthroplasty. Even though the optimal values for muscle elongation are not yet known, the measurement method allows an objective comparison of muscle elongations for different implant designs and positions, as well as patient anatomies. Furthermore, the method facilitates processing large data sets and investigating the impact of muscle elongations on postoperative outcomes.

Disclaimer

This work was supported by the Baekeland Scheme of the Flanders Agency for Innovation and Entrepreneurship (VLAIO) and by Marie Skłodowska-Curie Actions (grant no. 722535).

The authors, their immediate families, and any research foundations with which they are affiliated have not received any financial payments or other benefits from any commercial entity related to the subject of this article.

References

1. Berhouet J, Gulotta L, Chen X, Dines D, Warren R, Kontaxis A. Neutral glenoid alignment in reverse shoulder arthroplasty does not guarantee decreased risk of impingement. J Orthop Res 2018;36:1213-9. https://doi.org/10.1002/jor.23730
2. Bohsali KI, Bois AJ, Wirth MA. Complications of shoulder arthroplasty. J Bone Joint Surg Am 2017;99:256-69. https://doi.org/10.2106/JBJS.16.00935
3. Chae S-W, Kim S-Y, Lee H, Yon J-R, Lee J, Han S-H. Effect of baseplate size on primary glenoid stability and impingement-free range of motion in reverse shoulder arthroplasty. BMC Musculoskelet Disord 2014;15:417. https://doi.org/10.1186/1471-2474-15-417
4. Chalmers PN, Keener JD. Expanding roles for reverse shoulder arthroplasty. Curr Rev Musculoskelet Med 2016;9:40-8. https://doi.org/10.1007/s12178-016-9316-0
5. Cootes T. An introduction to active shape models. In: Image processing and analysis. Oxford: Oxford University Press; 2000. p. 223-48.

6. Danckaers F, Huysmans T, Lacko D, Ledda A, Verwulgent S, Van Dongen S, et al. Correspondence preserving elastic surface registration with shape model prior. In: 2014 22nd international conference on pattern recognition (ICPR). Piscataway, NJ: IEEE; 2014. p. 2143-8.
7. Dubrow S, Streit JJ, Muh S, Shishani Y, Gobezie R. Acromial stress fractures: correlation with acromioclavicular osteoarthritis and acromiohumeral distance. Orthopedics 2014;37:e1074-9. https://doi.org/10.3928/01477447-20141124-54
8. Frankle MA, Teramoto A, Luo Z-P, Levy JC, Pupello D. Glenoid morphology in reverse shoulder arthroplasty: classification and surgical implications. J Shoulder Elbow Surg 2009;18:874-85. https://doi.org/10.1016/j.jse.2009.02.013
9. Hamid N, Connor PM, Fleischli JF, D'Alessandro DF. Acromial fracture after reverse shoulder arthroplasty. Am J Orthop (Belle Mead NJ) 2011;40:125-9.
10. Hoenecke HR, Flores-Hernandez C, D'Lima DD. Reverse total shoulder arthroplasty component center of rotation affects muscle function. J Shoulder Elbow Surg 2014;23:1128-35. https://doi.org/10.1016/j.jse.2013.11.025
11. Holzbaur KRS, Murray WM, Delp SL. A model of the upper extremity for simulating musculoskeletal surgery and analyzing neuromuscular control. Ann Biomed Eng 2005;33:829-40. https://doi.org/10.1007/s10439-005-3320-7
12. Jobin CM, Brown GD, Bahu MJ, Gardner TR, Bigliani LU, Levine WN, et al. Reverse total shoulder arthroplasty for cuff tear arthropathy: the clinical effect of deltoid lengthening and center of rotation medialization. J Shoulder Elbow Surg 2012;21:1269-77. https://doi.org/10.1016/j.jse.2011.08.049
13. Kaptein BL, van der Helm FCT. Estimating muscle attachment contours by transforming geometrical bone models. J Biomech 2004;37:263-73. https://doi.org/10.1016/j.jbiomech.2003.08.005
14. Lädermann A, Denard PJ, Boileau P, Farron A, Deransart P, Walch G. What is the best glenoid configuration in onlay reverse shoulder arthroplasty? Int Orthop 2018;42:1339-46. https://doi.org/10.1007/s00264-018-3850-x
15. Lädermann A, Edwards TB, Walch G. Arm lengthening after reverse shoulder arthroplasty: a review. Int Orthop 2014;38:991-1000. https://doi.org/10.1007/s00264-013-2175-z
16. Marra MA, Vanheule V, Fluit R, Koopman BH, Rasmussen J, Verdonschot N, et al. A subject-specific musculoskeletal modeling framework to predict in vivo mechanics of total knee arthroplasty. J Biomech Eng 2015;137:020904. https://doi.org/10.1115/1.4029258
17. Matias R, Andrade C, Veloso AP. Accuracy of a transformation method to estimate muscle attachments based on three bony landmarks. Comput Methods Biomech Biomed Eng 2011;14:73-8. https://doi.org/10.1080/10255842.2010.499870
18. McFarland EG, Huri G, Hyun YS, Petersen SA, Srikumaran U. Reverse total shoulder arthroplasty without bone-grafting for severe glenoid bone loss in patients with osteoarthritis and intact rotator cuff. J Bone Joint Surg Am 2016;98:1801-7. https://doi.org/10.2106/JBJS.15.01181
19. Morgan SJ, Furry K, Parekh AA, Agudelo JF, Smith WR. The deltoid muscle: an anatomic description of the deltoid insertion to the proximal humerus. J Orthop Trauma 2006;20:19-21. https://doi.org/10.1097/01.bot.0000187063.43267.18
20. Mueller M, Hoy G. Soft tissue balancing in total shoulder replacement. Curr Rev Musculoskelet Med 2014;7:16-21. https://doi.org/10.1007/s12178-013-9195-6
21. Noothout JMH, de Vos BD, Wolterink JM, Leiner T, Išgum I. CNN-based landmark detection in cardiac CTA scans. In: Presented at the First Conference on Medical Imaging With Deep Learning; 2018. Amsterdam, The Netherlands.
22. Özmanevra R, Kaya E. Anterior deltoid insertion distance to various bony landmarks before and after humeral head lateralization. Acta Med Alanya 2019;3:17-20. https://doi.org/10.30565/medalanya.479819
23. Payer C, Štern D, Bischof H, Urschler M. Regressing heatmaps for multiple landmark localization using CNNs. In: Ourselin S, Joskowicz L, Sabuncu MR, Unal G, Wells W, editors. Medical image computing and computer-assisted intervention—MICCAI 2016. Cham: Springer International; 2016. p. 230-8.
24. Pellikaan P, van der Krogt MM, Carbone V, Fluit R, Vigneron LM, Van Deun J, et al. Evaluation of a morphing based method to estimate muscle attachment sites of the lower extremity. J Biomech 2014;47:1144-50. https://doi.org/10.1016/j.jbiomech.2013.12.010
25. Plessers K, Vanden Berghe P, Van Dijck C, Wirix-Speetjens R, Debeer P, Jonkers I, et al. Virtual reconstruction of glenoid bone defects using a statistical shape model. J Shoulder Elbow Surg 2018;27:160-6. https://doi.org/10.1016/j.jse.2017.07.026
26. Plessers K, Verhaegen F, Van Dijck C, Wirix-Speetjens R, Debeer P, Jonkers I, et al. Automated quantification of glenoid bone defects using 3-dimensional measurements. J Shoulder Elbow Surg 2020;29:1050-8. https://doi.org/10.1016/j.jse.2019.10.007
27. Redert A, Kaptein B, Reinders M, Van den Eelaart I, Hendriks E. Extraction of semantic 3D models of human faces from stereoscopic image sequences. Acta Stereol 1999;18:255-64.
28. Roche CP, Diep P, Hamilton M, Crosby LA, Flurin P-H, Wright TW, et al. Impact of inferior glenoid tilt, humeral retroversion, bone grafting, and design parameters on muscle length and deltoid wrapping in reverse shoulder arthroplasty. Bull Hosp Jt Dis 2013;71:284-93.
29. Salhi A, Burdin V, Mutsvangwa T, Sivarasu S, Brochard S, Borotikar B. Subject-specific shoulder muscle attachment region prediction using statistical shape models: a validity study. In: 2017 39th annual international conference of the IEEE Engineering in Medicine and Biology Society (EMBC). Piscataway, NJ: IEEE; 2017. p. 1640-3.
30. Saul KR, Hu X, Goehler CM, Vidt ME, Daly M, Velisar A, et al. Benchmarking of dynamic simulation predictions in two software platforms using an upper limb musculoskeletal model. Comput Methods Biomech Biomed Eng 2015;18:1445-58. https://doi.org/10.1080/10255842.2014.916698
31. Seim H, Kainmueller D, Heller M, Zachow S, Hege H-C. Automatic extraction of anatomical landmarks from medical image data: an evaluation of different methods. In: 2009 IEEE International Symposium on Biomedical Imaging: From Nano to Macro. Piscataway, NJ: IEEE; 2009. p. 538-41.
32. Sprengel R, Rohr K, Stiehl HS. Thin-plate spline approximation for image registration. In: Proceedings of 18th annual international conference of the IEEE Engineering in Medicine and Biology Society. Piscataway, NJ: IEEE; 1997. p. 1190-1.
33. Vanden Berghe P, Demol J, Gelaude F, Vander Sloten J. Virtual anatomical reconstruction of large acetabular bone defects using a statistical shape model. Comput Methods Biomech Biomed Eng 2017;20:577-86. https://doi.org/10.1080/10255842.2016.1265110
34. Victor J, Van Doninck D, Labey L, Innocenti B, Parizel PM, Bellemans J. How precise can bony landmarks be determined on a CT scan of the knee? Knee 2009;16:358-65. https://doi.org/10.1016/j.knee.2009.01.001
35. De Wilde L, Audenaert E, Barbaix E, Audenaert A, Soudan K. Consequences of deltoid muscle elongation on deltoid muscle performance: a computerised study. Clin Biomech 2002;17:499-505. https://doi.org/10.1016/S0268-0033(02)00065-7
36. Werthel J-D, Schoch BS, van Veen SC, Elhassan BT, An K-N, Cofield RH, et al. Acromial fractures in reverse shoulder arthroplasty: a clinical and radiographic analysis. 2018. J Shoulder Elbow Arthroplasty 2018;2:2471549218777628. https://doi.org/10.1177/2471549218777628
37. Wright J, Potts C, Smyth M, Ferrara L, Sperling J, Throckmorton T. A quantitative analysis of the effect of baseplate and glenosphere position on deltoid lengthening in reverse total shoulder arthroplasty. Int J Shoulder Surg 2015;9:33-7. https://doi.org/10.4103/0973-6042.154752
38. Zheng Y, Liu D, Georgescu B, Nguyen H, Comaniciu D. 3D deep learning for efficient and robust landmark detection in volumetric data. In: Navab N, Hornegger J, Wells WM, Frangi A, editors. Medical image computing and computer-assisted intervention—MICCAI 2015. Cham: Springer International; 2015. p. 565-72.